Soil Dynamics and Earthquake Engineering 30 (2010) 1361–1376

Contents lists available at ScienceDirect

Soil Dynamics and Earthquake Engineering

journal homepage: www.elsevier.com/locate/soildyn

Finite element analysis of buried steel pipelines under strike-slip fault displacements

Polynikis Vazouras [a], Spyros A. Karamanos [b,*], Panos Dakoulas [a]

[a] Department of Civil Engineering, University of Thessaly, Volos 38334, Greece
[b] Department of Mechanical Engineering, University of Thessaly, Volos 38334, Greece

ARTICLE INFO

Article history:
Received 3 February 2010
Received in revised form
16 June 2010
Accepted 24 June 2010

ABSTRACT

The present paper investigates the mechanical behavior of buried steel pipelines, crossing an active strike-slip tectonic fault. The fault is normal to the pipeline direction and moves in the horizontal direction, causing stress and deformation in the pipeline. The interacting soil–pipeline system is modelled rigorously through finite elements, which account for large strains and displacements, nonlinear material behavior and special conditions of contact and friction on the soil–pipe interface. Considering steel pipelines of various diameter-to-thickness ratios, and typical steel material for pipeline applications (API 5L grades X65 and X80), the paper focuses on the effects of various soil and pipeline parameters on the structural response of the pipe, with particular emphasis on identifying pipeline failure (pipe wall wrinkling/local buckling or rupture). The effects of shear soil strength, soil stiffness, horizontal fault displacement, width of the fault slip zone are investigated. Furthermore, the influence of internal pressure on the structural response is examined. The results from the present investigation are aimed at determining the fault displacement at which the pipeline fails and can be used for pipeline design purposes. The results are presented in diagram form, which depicts the critical fault displacement, and the corresponding critical strain versus the pipe diameter-to-thickness ratio. A simplified analytical model is also developed to illustrate the counteracting effects of bending and axial stretching. The numerical results for the critical strain are also compared with the recent provisions of EN 1998-4 and ASCE MOP 119.

1. Introduction

Earthquakes may constitute a threat for the structural integrity of buried pipelines. Post-earthquake investigations have demonstrated that the majority of seismic damages to continuous oil and gas steel pipelines were caused by permanent ground deformations such as fault movements, landslides, liquefaction-induced lateral spread, whereas only few pipelines were damaged by wave propagation [1] [2]. Permanent ground deformation is applied on the pipeline in a quasi-static manner, and it is not necessarily associated with high seismic intensity, but the pipeline may be seriously damaged. Such pipeline damages have been reported in numerous earthquakes, such as the 1971 San Fernando earthquake [3–5], and, more recently, the 1995 Kobe earthquake [6], the 1999 Kocaeli earthquake [7] and the 1999 Chi-Chi earthquake [8].

The present work examines the mechanical response of continuous (welded) buried steel pipelines crossing active strike-slip seismic faults. Those pipelines are subjected to an imposed deformation pattern, associated with axial, shear and bending loads, and develop high stresses and strains in critical locations, which are well into the inelastic range of pipe material and may cause pipeline failure. In particular, high tensile stresses may cause fracture of the pipeline wall, especially at welds or defected locations or welds, whereas high compression stresses may cause buckling, either in the form of beam-type (global) instability or in the form of pipe wall wrinkling, a shell-type instability, sometimes referred to as "local buckling" or "kinking".

To assess pipeline strength against an imposed strike-slip fault displacement, the distribution of stress and strain within the pipeline wall should be calculated for the imposed deformation. The work of Newmark and Hall [9] was the first attempt to predict pipeline mechanical response under fault displacement, using a simplified analytical model of a long cable with small displacements, which relates the soil slip friction on the pipe directly to the earth static pressure. This work has been extended by Kennedy et al. [10] and Kennedy and Kincaid [11] considering non-uniform friction between the pipe and the surrounding soil. This methodology was enhanced by Wang and Yeh [12] to account for pipeline bending stiffness. Vougioukas et al. [13]

* Corresponding author.
E-mail addresses: skara@uth.gr (S.A. Karamanos), dakoulas@uth.gr (P. Dakoulas).

0267-7261/$ - see front matter © 2010 Elsevier Ltd. All rights reserved.
doi:10.1016/j.soildyn.2010.06.011

considered both horizontal and vertical movement of faults and numerically analyzed buried pipes as elastic beams. In later publications, McCaffrey and O'Rourke [4] and Desmod et al. [5] studied the development of strains in buried pipes crossing faults based on the performance of gas and water pipes during the San Fernando earthquake. Wang and Wang [14] studied the same problem considering the pipe as a beam on elastic foundation, whereas Takada et al. [15] presented a new simplified method for evaluating the critical strain of the fault crossing steel pipes using the relation between pipe-deformation (geometry) at longitudinal direction with sectional large deformation.

In a recent paper, Kokavessis and Anagnostidis [16] presented a finite element methodology to simulate buried pipeline behavior under permanent ground-induced actions, using contact elements to describe the soil–pipe interaction. Furthermore, an analytical methodology was presented by Karamitros et al. [17], which introduced a number of refinements in existing methodologies. The axial force and the bending moment on the pipeline are obtained through a combination of beam-on-elastic-foundation and elastic-beam theory, considering material and geometric nonlinearities to calculate the maximum design strain. The analytical predictions are compared with three-dimensional finite element models, which employed a coarse shell element mesh for describing the pipe and nonlinear springs to simulate soil behavior. More recently, Liu et al. [18] presented a numerical simulation of pipelines crossing active faults through a shell finite element model, similar to the model in [17] (i.e. a combination of shell elements and springs), and reported results for the distribution of axial strain along the pipeline.

In addition to the above numerical studies, notable experimental works on the effects of strike-slip faults on buried high-density polyethylene (HDPE) pipelines have been reported in series of recent papers by Ha et al. [19,20] and Abdoun et al. [21]. This experimental investigation was based on centrifuge modeling of pipeline response to seismic faulting. The tests examined the influence of the type of faulting, the angle of strike-slip faults on the pipeline mechanical behavior, as well as the effects of buried depth and pipeline diameter, and moisture content.

The work described in the present paper is part of an extensive research effort aimed at investigating the mechanical behavior of buried steel pipelines crossing active faults for various soil conditions, using advanced numerical simulation tools and identifying possible failure modes. It has been recognized that, apart from the geometric and mechanical properties of the steel pipeline, site conditions (i.e. the properties of the surrounding soil) may have a strong influence on pipeline response [22]. The present work follows an integrated approach, which is based on modeling of the soil–pipeline system through nonlinear finite elements, accounting rigorously for (a) the inelastic behavior of the surrounding soil, (b) the interaction and the contact between the soil and the pipe (including friction contact and the development of gap), (c) the development of large inelastic strains in the steel pipeline, (d) the distortion of the pipeline cross-section and possible local buckling formation and (e) the presence of internal pressure. The pipeline axis is assumed horizontal and normal to the fault plane, which is an idealized case, allowing for the direct investigation of the influence of several material and geometric parameters on pipeline mechanical behavior. Considering a variety of soil parameters for both cohesive and non-cohesive soils, the influence of soil conditions on the pipeline structural response is examined in detail. Furthermore, the effects of pipeline diameter-to-thickness ratio D/t and steel material stress–strain curve are also investigated.

For each case of soil conditions and pipeline geometry/material characteristics, the shape of the deformed pipe is obtained, including local distortion or buckling of its cross-section. Numerical

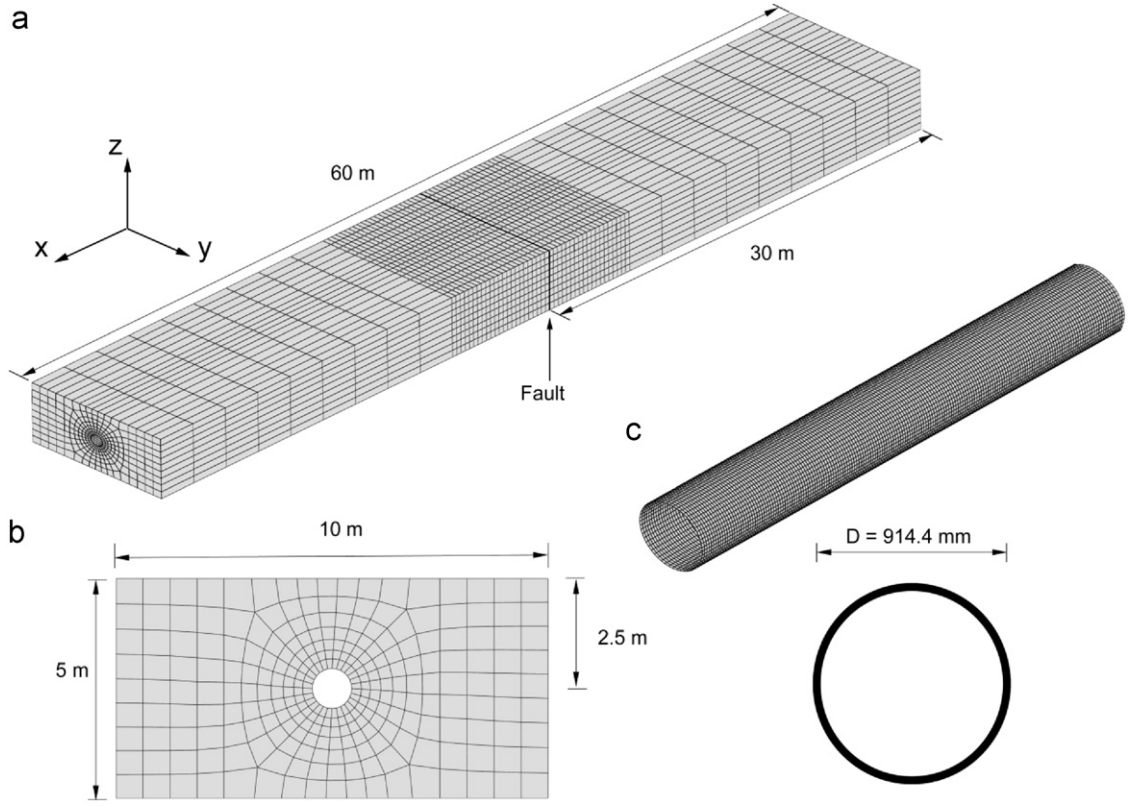

Fig. 1. Finite element model of the (a) soil formation with tectonic fault, (b) soil cross-section, and (c) steel pipeline.

results are presented in terms of the axial strain along the pipeline outer generators, so that the critical strain that causes local buckling is computed and compared with the corresponding strain used in current design practice. Results for the maximum tensile strain are also obtained, which is also compared with the corresponding allowable value specified in existing design specifications. Finally, the numerical results are employed to develop interaction diagrams of the fault displacement causing pipeline failure with respect to the value of pipe diameter-to-thickness ratio D/t, which could be used for practical design purposes.

2. Numerical modeling

The structural response of steel pipelines under fault movement is examined numerically using advanced computational tools. General-purpose finite element program ABAQUS [23] is employed to simulate the mechanical behavior of the steel pipe, the surrounding soil medium and their interaction in a rigorous manner, considering the nonlinear geometry of the soil and the pipe (including the distortions of the pipeline cross-section), through a large-strain description of the pipeline–soil system and the inelastic material behavior for both the pipe and the soil.

An elongated prismatic model is considered (Fig. 1), where the pipeline is embedded in the soil. The corresponding finite element mesh for the soil formation is depicted in Fig. 1a and b, and for the steel pipe in Fig. 1c. Four-node reduced-integration shell elements (type S4R) are employed for modeling the pipeline cylinder, whereas eight-node reduced-integration "brick" elements (C3D8R) are used to simulate the surrounding soil. The top surface represents the soil surface, and the burial depth is chosen equal to

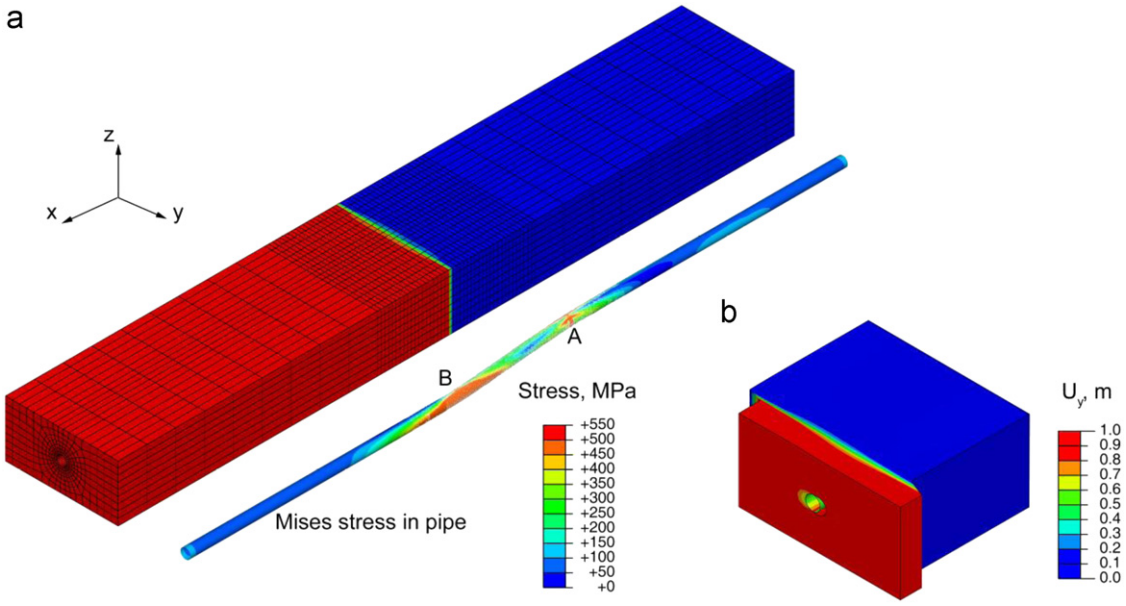

Fig. 2. (a) Deformation of the pipeline–soil system after fault displacement; finite element results depict the von Mises stress. (b) Detail of fault displacement U_y, illustrating the development of a gap opening at the soil–pipe interface (X65 pipe, $D/t=72$, Clay I, $w=0.33$ m, $p=0$).

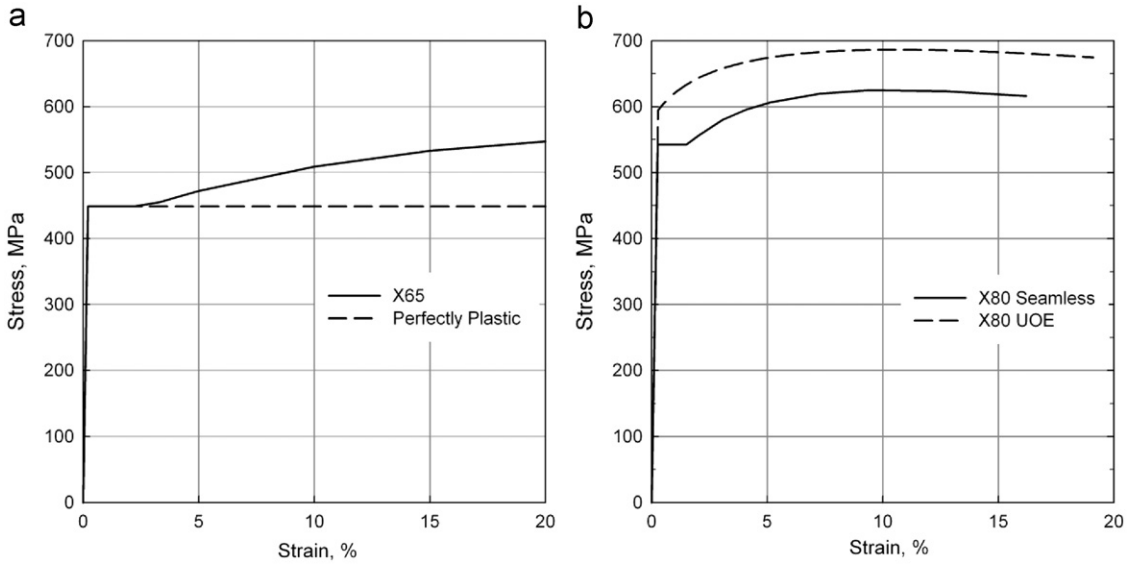

Fig. 3. Uniaxial nominal stress-engineering strain curve (a) API 5L X65 steel; (b) API 5L X80 steel.

about 2 pipe diameters, which is in accordance with pipeline engineering practice [24]. A short parametric study demonstrated that a 60-diameter length of the pipeline (in the x direction) is adequate for the purposes of the present analysis. Furthermore, prism dimensions in directions y and z equal to 10 and 5 times the pipe diameter, respectively, are also found to be adequate. The seismic fault plane is considered perpendicular to the pipeline axis at the pipeline middle section and divides the soil in two equal parts (Fig. 1a). The analysis is conducted in two steps: gravity loading is applied first and, subsequently, fault movement is imposed. The vertical boundary nodes of the first block remain fixed in the horizontal direction (including the end nodes of the steel pipeline), whereas a uniform displacement due to fault movement is imposed in the external nodes of the second (moving) block in the horizontal y direction (including the end nodes of the pipeline). A fine mesh was employed for the central part of the pipeline, where maximum stresses and strains are expected. Following a short parametric study, a total of 54 shell elements around the cylinder circumference in this central part have been found to be adequate to achieve convergence of solution, whereas the size of the shell elements in the longitudinal direction has been chosen equal to 1/26 of the pipeline outer diameter D. On the other hand, a coarser mesh was chosen for the pipe parts far from the fault location. Similarly, the finite element mesh for the soil is more refined in the region near the fault and coarser in the region away from the fault.

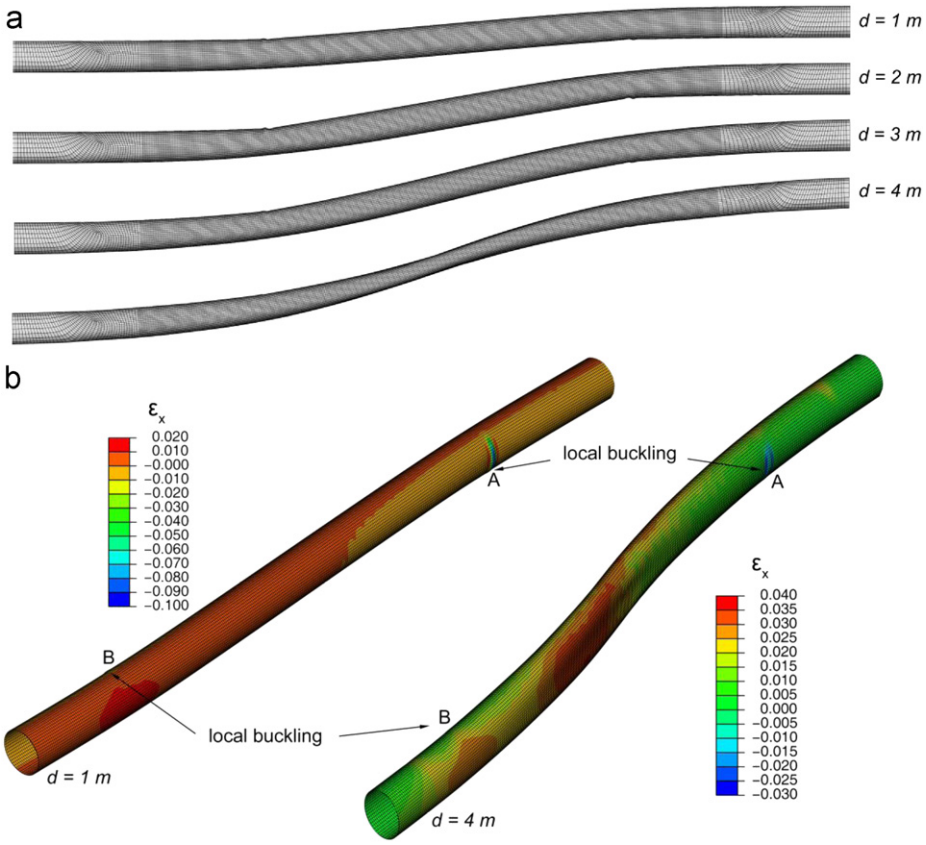

Fig. 4. (a) Plan view of deformed shape of a pipeline for $d=1$–4 m and (b) distribution of longitudinal normal strain ε_x for seismic fault displacement equal to 1 and 4 m (X65 pipe, $D/t=72$, Clay I, $w=0.33$ m, $p=0$).

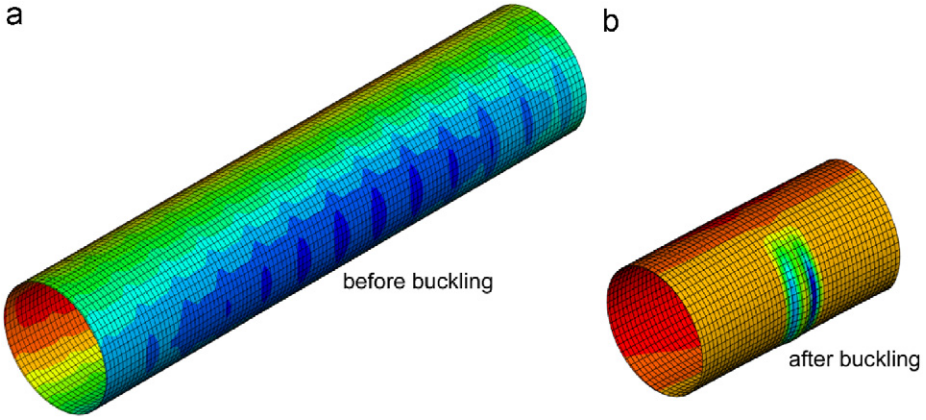

Fig. 5. Details of the critical pipeline area: (a) transition from a smooth configuration to a wavy pattern, which is quasi-uniform along the pipeline; (b) local buckling formation (X65 pipe, $D/t=72$, Clay I, $w=0.33$ m, $p=0$).

Fig. 2a plots the soil–pipeline system after a seismic fault movement in the y direction. The fault movement is considered to occur within a narrow transverse zone of width w, a common practice in several recent numerical studies of fault–foundation interaction [25,26]. Using this approach, it is possible to avoid discontinuity at the vicinity of the fault, which sometimes causes numerical problems. Furthermore, this consideration may correspond to a more realistic representation of the fault displacement mechanism, as demonstrated in small scale model tests [27]. The sensitivity of numerical results with respect to the width w of that narrow zone is examined in a subsequent section of the paper.

Elastic–plastic material behavior is considered for both the pipeline and soil. A large-strain J_2 flow (von Mises) plasticity model with isotropic hardening is employed to describe the mechanical behavior of the steel pipe material, calibrated through an appropriate uniaxial stress–strain curve from a tensile test. Furthermore, an elastic–perfectly plastic Mohr–Coulomb model is considered for the soil behavior, characterized by the soil cohesiveness c, the friction angle φ, the elastic modulus E, and Poisson's ratio ν. The dilation angle ψ is assumed to be equal to zero throughout this study.

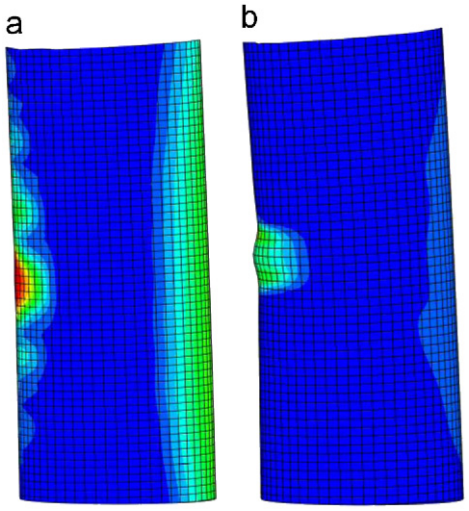

Fig. 6. Variation of equivalent plastic shear strain at the critical pipeline area: (a) transition from a smooth configuration to a uniform wavy pattern and (b) local buckling formation (X65 pipe, $D/t=72$, Clay I, $w=0.33$ m, $p=0$).

A contact algorithm is considered to simulate the interface between the outer surface of the steel pipe and the surrounding soil. The algorithm takes into account interface friction, which is considered through definition of an appropriate friction coefficient μ. In our analysis, the value of μ is equal to 0.3. It is worth noticing that, following a short parametric study, variation of the value of μ between 0.2 and 0.4 had a rather small effect on the numerical results. Moreover, the interface allows separation of the pipe and the surrounding soil. Fig. 2b illustrates clearly the local separation of the pipe and the soil after some fault displacement.

The analysis proceeds using a displacement-controlled scheme, which increases gradually the fault displacement d. At each increment of the nonlinear analysis, stresses and strains at the pipeline wall are recorded. Furthermore, due to the fine mesh employed at the critical pipeline portions, local buckling (wrinkling) formation and post-buckling deformation at the compression side of the pipeline wall are simulated in a rigorous manner.

3. Numerical results

Using the above numerical simulation tools, results are obtained for steel pipelines for various values of the diameter-to-thickness ratio, as well as for different soil conditions. In all cases considered in the present paper, the outer pipe diameter of pipe D is assumed equal to 914.4 mm (36 in.), whereas the pipe wall thickness ranges from 6.35 mm (1/4 in.) to 19.05 mm (3/4 in.), so that a range of D/t values between 48 and 144 is covered. This range of D/t values is typical for onshore applications (oil, gas or water pipelines). The surrounding soil has dimensions 60 m × 10m × 5 m in directions x, y, z, respectively. The seismic fault plane is perpendicular to the pipeline axis and located at the middle cross-section of the pipeline.

In Sections 3.1 and 3.2, steel pipelines with API 5L [28] X65 steel material and thickness equal to 12.7 mm (0.5 in.) are examined under cohesive and non-cohesive soil conditions, respectively, using appropriate values of soil parameters c, ϕ, and E. The influence of fault width w on the pipeline response is examined, as well as the effects of internal pressure. In addition, the influence of steel material hardening on the structural response and the failure mode is investigated. Subsequently, in Section 3.3, X65 pipelines with different values of the diameter-to-thickness ratio D/t are analyzed, to identify the influence of the diameter-to-thickness ratio on the structural

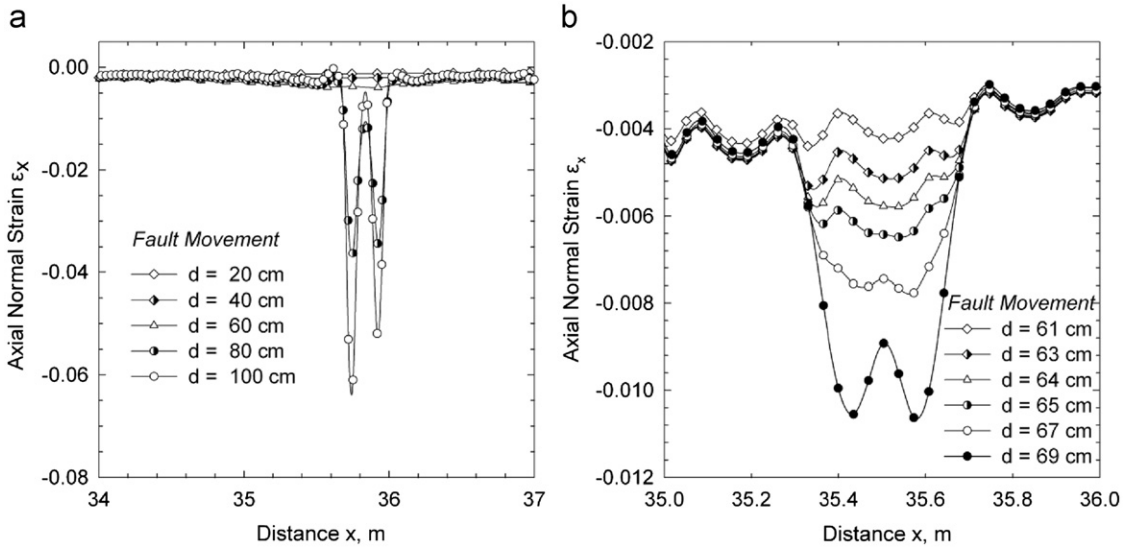

Fig. 7. Variation of axial strain at the compression side of the buckled area for different values of fault displacement: (a) fault movement from 0.2 to 1.0 m and (b) fault movement from 0.61 to 0.69 m (X65 pipe, $D/t=72$, Clay I, $w=0.33$ m, $p=0$).

response. Finally, high-strength steel X80 pipelines under fault imposed deformations are analyzed in Section 3.4.

3.1. Moderately thick X65 steel pipeline in cohesive soils

A moderately thick-walled X65 pipeline is considered first, with diameter and thickness equal to 914.4 mm (36 in.) and 12.7 mm (0.5 in.), respectively, so that $D/t=72$. The API 5L X65 steel material is a typical steel material for oil and gas pipeline applications, with a nominal stress-engineering strain curve shown with a solid line in Fig. 3a, obtained from a uniaxial tensile test. The yield stress σ_y is equal to 450 MPa (65 ksi) followed by a plastic plateau up to 3% strain and a strain-hardening regime with a hardening modulus equal to about $E_s/300$, where E_s is Young's modulus of the steel material. Considering a safety (reduction) factor equal to 0.72 [29,30], the maximum operating pressure p_{max} of this pipeline, given by the following expression:

$$p_{max}=0.72\times\left(2\sigma_y\frac{t}{D}\right) \tag{1}$$

can be readily calculated equal to 9 MPa (90 barr).

The pipeline is assumed to be imbedded in a cohesive soil and to be crossing a fault zone having a width w equal to 0.33 m. Its internal pressure p is equal to zero, but it is increased subsequently in the present study. First, a soft-to-firm clay is considered, referred to as Clay I, which under "undrained" loading conditions has a cohesion $c=50$ kPa, friction angle $\varphi=0^\circ$, Young's modulus $E=25$ MPa and Poisson's ratio $v=0.5$.

Fig. 4a depicts the shape of the deformed pipeline at fault displacements $d=1$–4 m in the area near the fault. Moreover, Fig. 4b plots depict the shape of the deformed pipeline and the distribution of the longitudinal normal strain ε_x on its outer surface at fault displacement equal to $d=1$ and $d=4$ m. The deformed shape of the pipeline at $d=1$ m shows a localized deformation at point A, referred to as "local buckling" or "kinking", whereas point A is the "critical location" of the pipeline, at a distance of 5.45 m from the fault. Due to the skew-symmetry of the problem, a similar local deformation pattern occurs at point B, on the hidden side of the pipeline. Under increasing fault movement, a substantial development of this localized deformation pattern is observed, associated with the distortion of a significant part of the pipeline around this area, as shown in Fig. 4b, for a fault displacement of $d=4$ m. As the pipeline length increases with continued fault movement, it results in higher tensile and smaller compressive strains in the longitudinal direction. This is shown in Fig. 4b, where for a fault displacement of $d=4$ m compressive longitudinal strains are significantly lower than those corresponding to a fault displacement of $d=1$ m. The overtaking of the tensile strains after some critical value of d is discussed later in the paper.

Fig. 5 shows two consecutive deformed shapes of the pipeline at fault displacements d equal to 0.2 and 1 m, whereas Fig. 6 plots the same deformed shapes in a plan view. The localized buckling pattern depicted in Figs. 5 and 6 develops on the critical location along the pipeline, where the compressive stresses and strains, and the corresponding bending curvature reach a maximum value. It is interesting to note that the buckled shape of the compressed wall is formed in two stages. First a transition from a

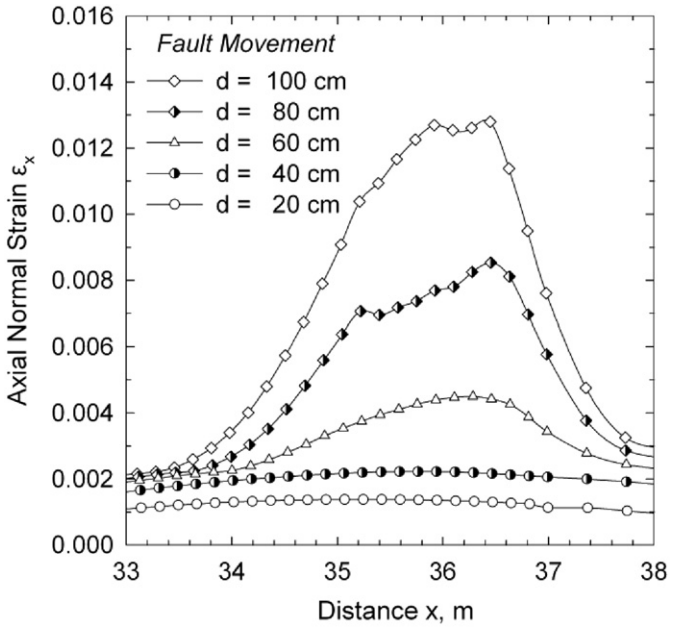

Fig. 8. Variation of axial strain at the tension side of the buckled area for values of fault displacement from 0.2 to 1.0 m (X65 pipe, $D/t=72$, Clay I, $w=0.33$ m, $p=0$).

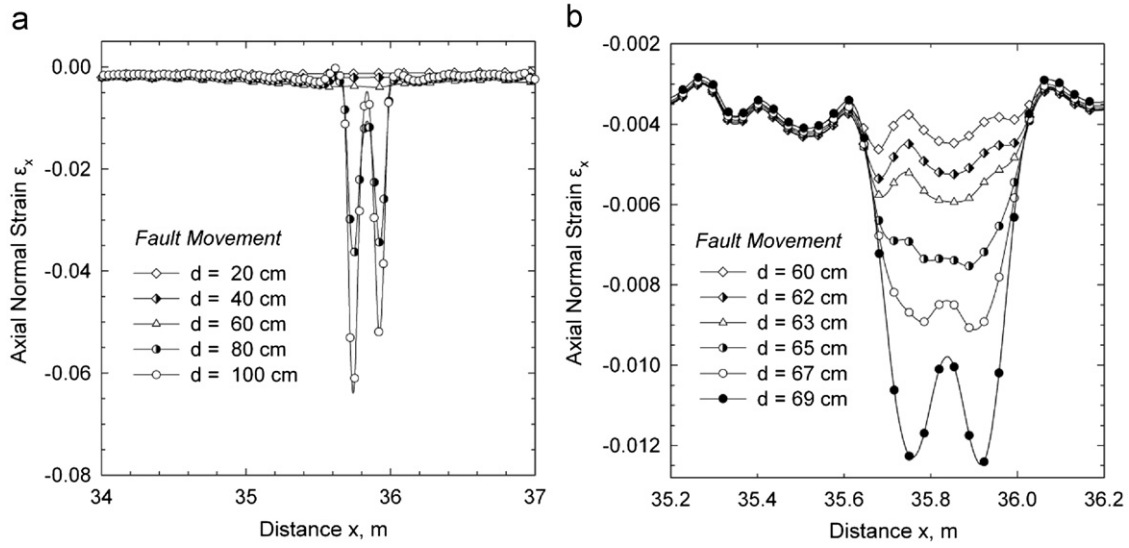

Fig. 9. Variation of axial strain at the compression side of the buckled area for different values of fault displacement: (a) fault movement from 0.2 to 1.0 m and (b) fault movement from 0.60 to 0.69 m (X65 pipe, $D/t=72$, Clay I, $w=1$ m, $p=0$).

"smooth" deformation shape to a "wavy" pattern occurs, in the form of quasi-uniform wrinkling along a certain part of the pipeline about the critical cross-section, as shown clearly in Fig. 5a. Subsequently, one of the wrinkles becomes dominant and the deformation localizes ("buckle localization"), forming a sharp "kink" or "local buckle", depicted in Fig. 5b. This mechanism of buckle initiation and localization is in accordance with previous experimental observations in metal cylinders subjected to bending [31,32]. It is also important to notice that, upon local buckling formation, the deformation of the pipeline localizes in the vicinity of the buckle, as shown in Fig. 5b. The variations of longitudinal compressive and tensile strain ε_x along the two outer (most stressed) generators of the pipe cylinder are shown in Figs. 7 and 8 for different values of the fault displacement and for a small segment of the pipeline about the critical area. The results for the compressive strain shown in detail in Fig. 7b indicate that for a value of fault displacement greater than 0.67 m, significant distortion of the cross-section occurs due to the development of a localized wrinkling pattern (local buckling) on the pipe wall, on the compression side of the deformed pipeline. This stage is considered as the onset of local buckling.

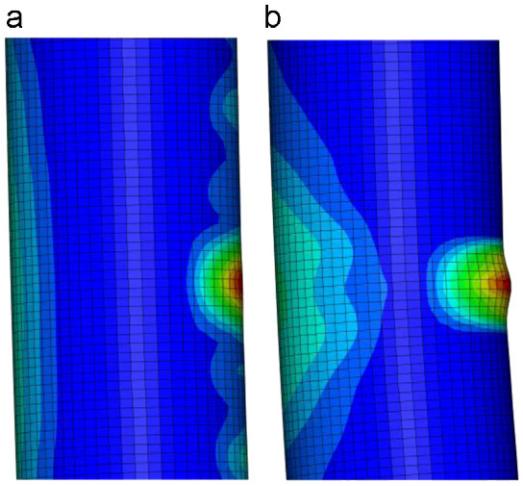

Fig. 10. Variation of equivalent plastic shear strain at the critical pipeline area: (a) transition from a smooth configuration to a uniform wavy pattern and (b) local buckling formation (X65 pipe, $D/t=72$, Clay I, $w=0.33$ m, $p=0.56p_{max}$).

It should be noted that determining the value of fault displacement at which onset of localized buckling occurs (d_{cr}), referred to as "critical fault displacement", can be defined in many ways. In the present work, the onset of local buckling is considered at the stage where outward displacement of the pipe wall starts at the area of maximum compression. At that stage, bending strains due to pipe wall wrinkling develop (Fig. 7), associated with significant tensile strains at the "ridge" of the buckle, so that the longitudinal compressive strains at this location at the outer surface of the pipe wall start decreasing, forming a short wave at this location. In the present case, this stage corresponds to a fault displacement equal to 0.67 m as shown in Fig. 7b.

At the above stage of local buckling onset, the longitudinal strain at the location of the buckle (ε_{cr}) is measured equal to 7.7×10^{-3}. Furthermore, at this critical buckling stage, the

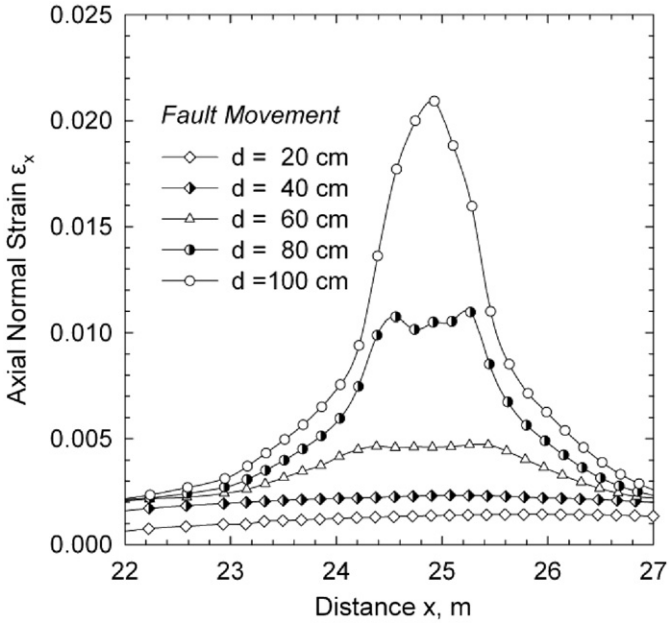

Fig. 12. Variation of axial strain at the tension side of the buckled area for different values of fault displacement from 0.2 to 1.0 m (X65 pipe, $D/t=72$, Clay I, $w=0.33$ m, $p=0.56p_{max}$).

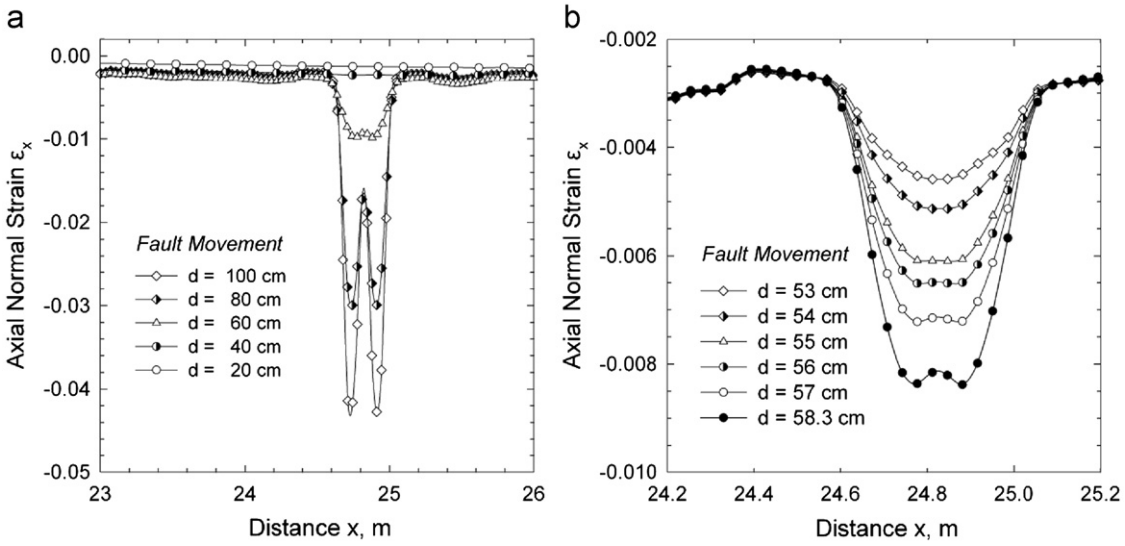

Fig. 11. Variation of axial strain at the compression side of the buckled area for different values of fault displacement: (a) fault movement from 0.2 to 1.0 m and (b) fault movement from 0.53 to 0.58 m (X65 pipe, $D/t=72$, Clay I, $w=0.33$ m, $p=0.56p_{max}$).

maximum tensile strain on the opposite side of the pipe ($\varepsilon_{T,\,max}$) is 5.2×10^{-3}, which is much less than the strain that would cause tensile failure in the form of rupture in a non-seriously defected pipeline [34,35]. Beyond the formation of the local buckle, pipe deformation concentrates around the buckled cross-section, and the localized wrinkling pattern is significantly developed. Further continuation of the imposed deformation results in pipe wall folding, which is accompanied by significant local strains (compressive and tensile) at the buckled area. Similarly, the maximum tensile strain on the opposite (tensile) side of the pipe is also significantly increased. Those local tensile stresses, on either side of the pipeline cross-section, may lead to local fracture at welds or other locations where minor defects exist, resulting in loss of pipeline containment with possibly catastrophic consequences for the population and the environment.

The effects of the size of fault zone w on the mechanical response of the pipeline are also examined. Finite element analyses have been conducted for several values of w ranging from 0.33 to 1.0 m. The numerical results indicated that that the width of the fault zone w has a minor effect on the response of the pipeline; this can be readily verified by comparing the results of Fig. 9 with those depicted in Fig. 7.

The effects of internal pressure on pipeline mechanical behavior are investigated by considering internally pressurized pipelines imbedded in the same soil conditions (Clay I). The numerical results presented in Fig. 10–12 correspond to a pressure level of 50 barr, which is equal to 56% of the maximum operating pressure p_{max} expressed by Eq. (1), whereas the results in Figs. 13–15 refer to a pressure level of 25 barr, which is equal to 28% of p_{max}. Despite the fact that the buckled shapes shown in Fig. 10 and in Fig. 13 are similar to the buckled shape of Fig. 6, the corresponding values of critical fault displacement d_{cr} and the compressive strain along the critical generator of the steel pipeline shown in Fig. 11b and in Fig. 14b are lower than the ones shown in Fig. 7b. These results indicate that, in the case of buried (confined) pipes, the presence of internal pressure results in a decrease of critical fault displacement. The decrease is attributed to the development of additional stresses and strains in the pipeline wall that cause early yielding and lead to a premature local buckling failure. This implies a different structural behavior

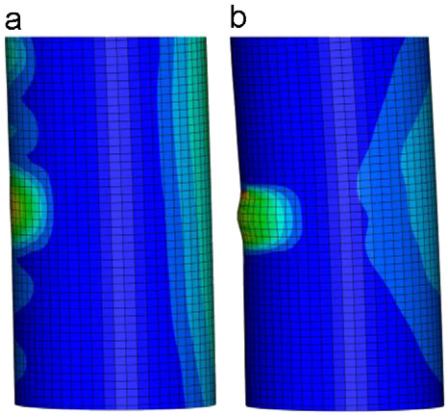

Fig. 13. Variation of equivalent plastic shear strain at the critical pipeline area: (a) transition from a smooth configuration to a uniform wavy pattern and (b) local buckling formation (X65 pipe, $D/t=72$, Clay I, $w=0.33$ m, $p=0.28p_{max}$).

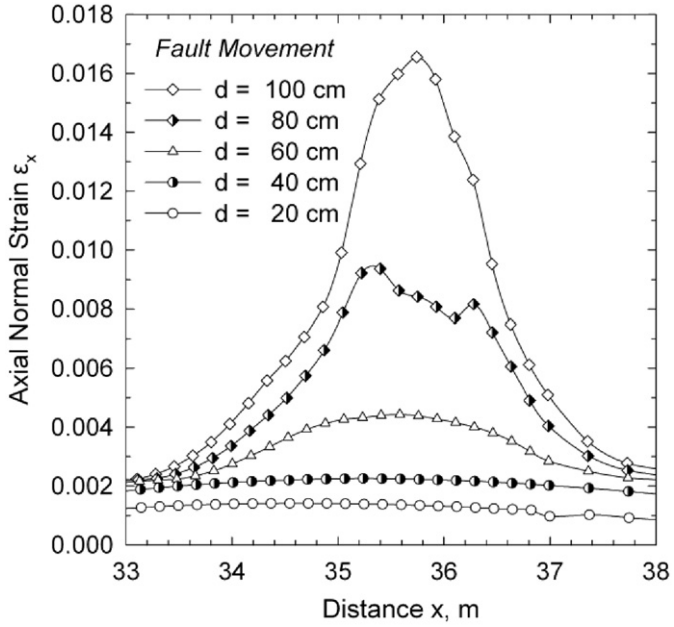

Fig. 15. Variation of axial strain at the tension side of the buckled area for different values of fault displacement from 0.2 to 1.0 m (X65 pipe, $D/t=72$, Clay I, $w=0.33$ m, $p=0.28p_{max}$).

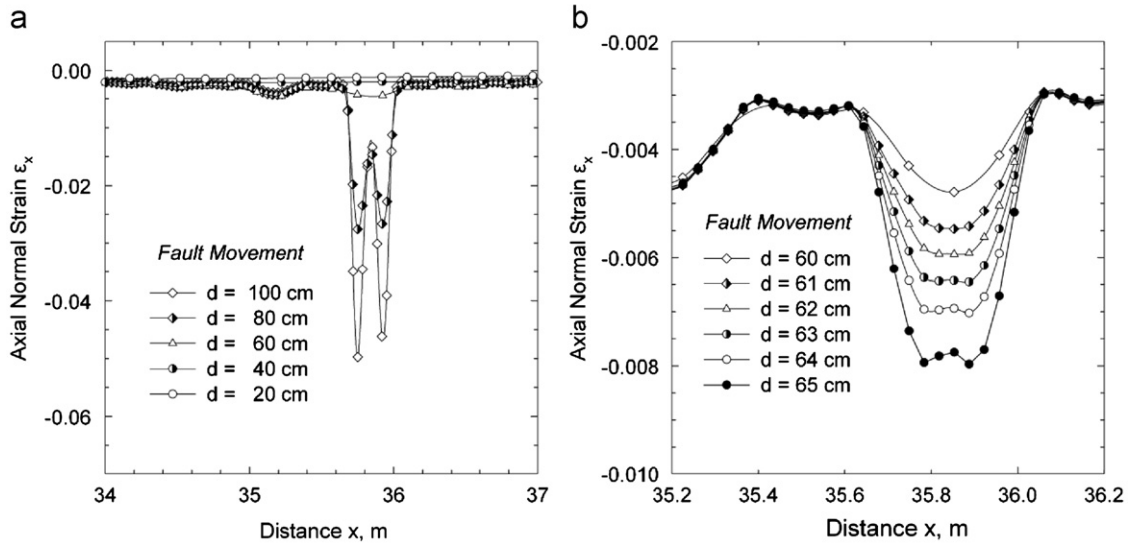

Fig. 14. Variation of axial strain at the compression side of the buckled area for different values of fault displacement: (a) fault movement from 0.2 to 1.0 m and (b) fault movement from 0.60 to 0.65 m (X65 pipe, $D/t=72$, Clay I, $w=0.33$ m, $p=0.28p_{max}$).

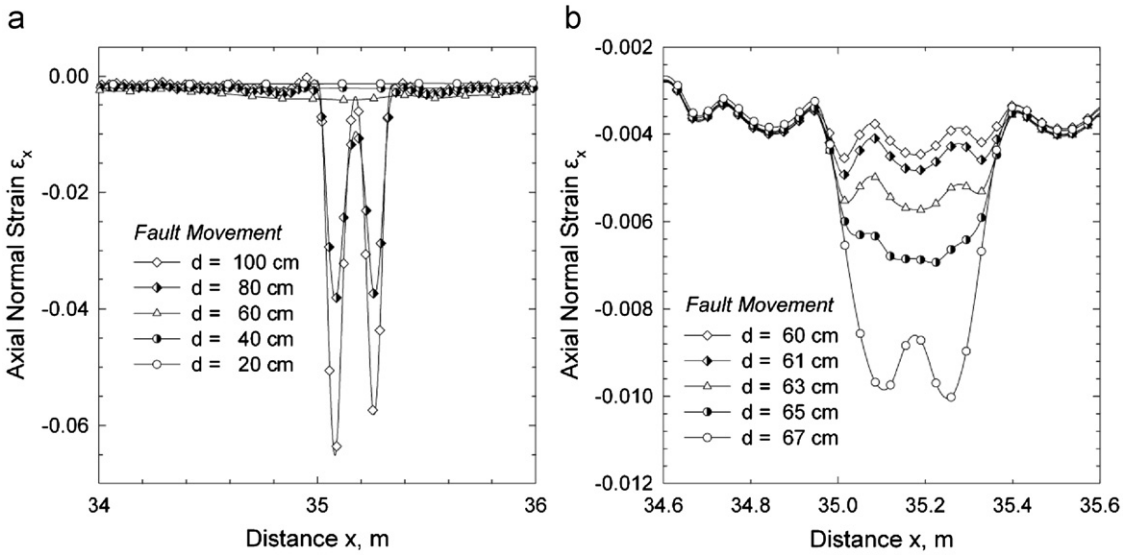

Fig. 16. Variation of axial strain at the compression side of the buckled area for X65 steel with no hardening: (a) fault movement from 0.2 to 1.0 m and (b) fault movement from 0.60 to 0.67 m ($D/t=72$, Clay I, $w=0.33$ m, $p=0$).

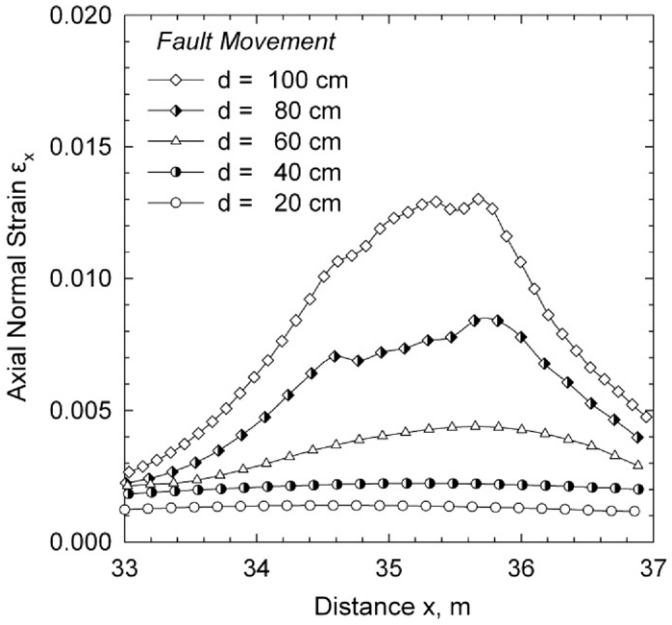

Fig. 17. Variation of axial strain at the tension side of the buckled area for X65 steel with no hardening and different values of fault displacement from 0.2 to 1.0 m ($D/t=72$, Clay I, $w=0.33$ m, $p=0$).

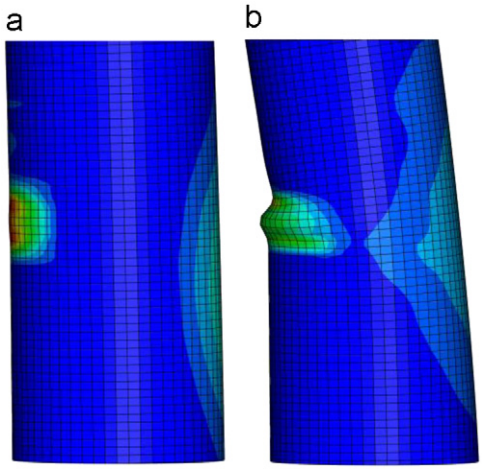

Fig. 18. Variation of equivalent plastic shear strain at the critical pipeline area: (a) onset of local buckling and (b) post-buckling configuration (X65 pipe, $D/t=72$, Clay II, $w=0.33$ m, $p=0$).

than the one observed in bending tests of laterally unconfined pipes [31,33], due to the presence of surrounding soil that has a significant confinement effect. For the case of $p/p_{max}=0.56$, the maximum strain ε_{cr} at buckling (critical strain) is equal to 8.3×10^{-03}, which is similar yet slightly higher than the critical strain for zero pressure.

The structural response of the same steel pipeline is shown in Fig. 16 and in Fig. 17 considering an elastic–plastic material of 450 MPa yield stress (same as in X65) but with perfect plasticity (no hardening). The stress–strain curve of this material is plotted with the dotted line in Fig. 3a. The values of soil parameters c, E, and ϕ are equal to 50 kPa, 25 MPa, and 0°, respectively (Clay I). The critical fault displacement has been computed equal to 67 cm. Comparison of those results with the results in Figs. 7 and 8 indicates that the hardening of the steel material has a negligible influence on the structural response of the pipeline subjected to strike-slip fault displacement perpendicular to the pipeline axis.

The numerical results in Figs. 18–20 refer to an X65 steel pipeline with D/t ratio equal to 72, buried in stiffer cohesive soil conditions. The values of soil parameters c, E, and ϕ are equal to 200 kPa, 100 MPa, and 0°, respectively, and correspond to a stiff clay under "undrained conditions", referred to as Clay II. The width of the fault zone is equal to 0.33 m. The numerical results indicate that pipe bending deformation in the stiff soil occurs within a shorter distance from the fault location, and the critical area is at 3.2 m from the fault. Comparison of those results with the results shown in Figs. 6–8 demonstrates the significant effect of site conditions on the mechanical behavior of the steel pipeline. In other words, for the same fault displacement d, higher bending stresses and strains occur in the case of a stiff soil than those in the case of a soft soil. The numerical verification of the above observation is offered in Figs. 19 and 20, which depict the variation of longitudinal (axial) normal strain along the compression generator. Local buckling occurs when the fault displacement becomes equal to 0.23 m, which is much less than the corresponding critical fault displacement for the case of soft clay (0.67 m). The corresponding maximum

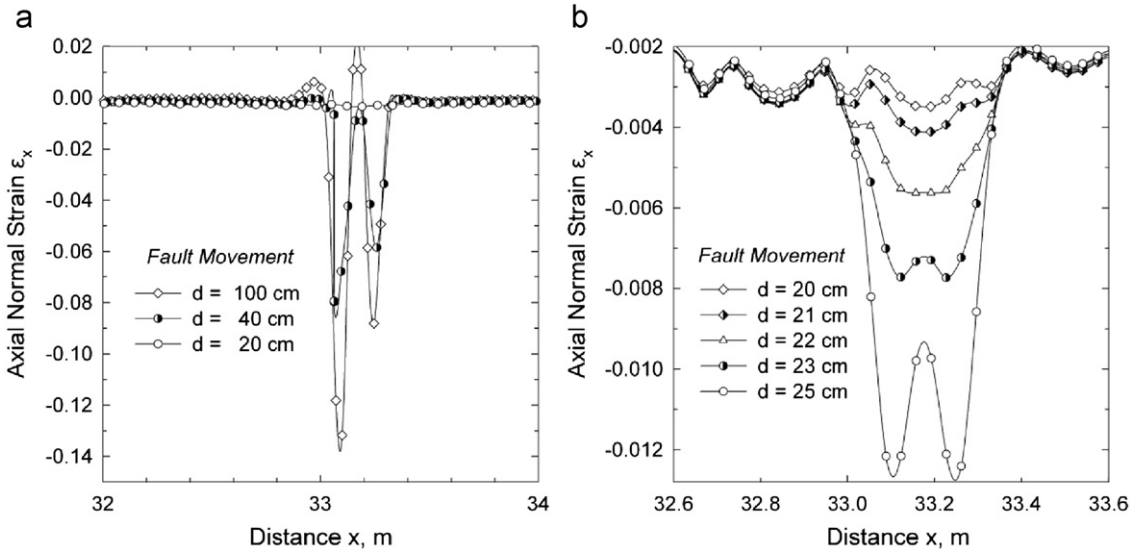

Fig. 19. Variation of axial strain at the compression side of the buckled area for different values of fault displacement: (a) fault movement from 0.2 to 1.0 m and (b) fault movement from 0.20 to 0.25 m (X65 pipe, $D/t=72$, Clay II, $w=0.33$ m, $p=0$).

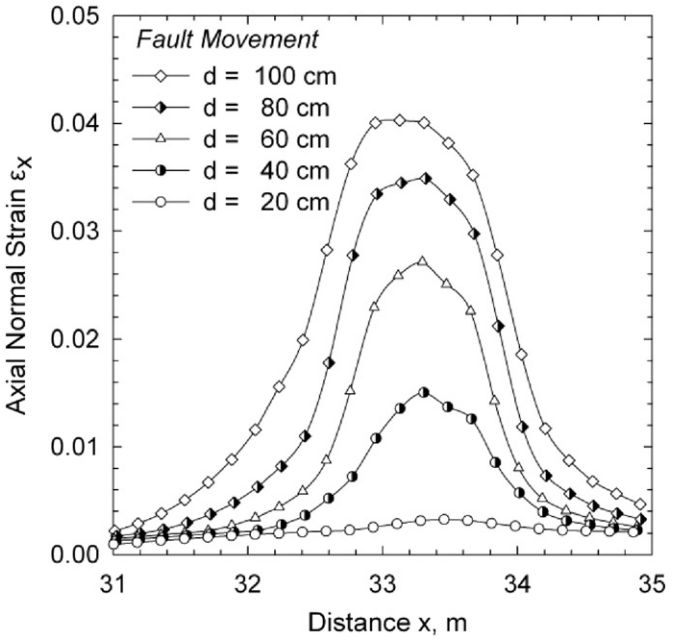

Fig. 20. Variation of axial strain at the tension side of the buckled area for different values of fault displacement from 0.2 to 1.0 m (X65 pipe, $D/t=72$, Clay II, $w=0.33$ m, $p=0$).

compressive strain ε_{cr} that causes local buckling is equal to 7.3×10^{-3}, whereas the maximum tensile strain $\varepsilon_{T,\ max}$ along the opposite generator at the stage of local buckling onset is equal to 4.8×10^{-3}. The striking difference between softer and stiffer soil conditions is attributed to the fact that a steel pipeline in a softer soil, when subjected to a fault displacement, accommodates itself easier within the deformable soil, resulting in lower bending stresses and strains, which enable the pipeline to sustain larger ground-imposed displacements.

3.2. Moderately thick X65 steel pipeline in non-cohesive soils

The response of an X65 steel pipeline with $D/t=72$ embedded in non-cohesive soils is examined, by considering representative results for two frictional soils and comparing them to those obtained for the cohesive soils. First, a granular soil is considered with a friction angle $\phi=30^\circ$, Young's modulus $E=8$ MPa and Poisson's ratio $\nu=0.3$, corresponding to loose sand and referred to as "Sand I". The relatively small value of the stress-depended Young's modulus E is justified by the shallow embedment depth of the pipeline. A small amount of artificial cohesion equal to $c=5$ kPa was also included to prevent numerical difficulties associated with the behavior of a purely frictional material at very small confining stress, such as in the case of a gap opening at the pipe–soil interface. Figs. 21 and 22 show the variation of the axial strain ε_x along the compression and tension outer sides, respectively, of the buckled area for Sand I. The critical distance from the fault, corresponding to the point with maximum bending curvature along the pipe, is 6.1 m. The results for the compressive strain shown in Fig. 21 indicate that at a value of fault displacement equal to 0.87 m, local buckling occurs, and beyond this stage, significant distortion of the cross-section occurs due to local buckling on the pipe wall on the compression side of the bent pipeline. The shape of the developing buckling is similar to that of Clay I. The longitudinal strain at the location of the buckle (ε_{cr}) is equal to 9.7×10^{-3}. Furthermore, at the critical buckling stage ($d=0.87$ m), the maximum tensile strain on the opposite side of the pipe ($\varepsilon_{T,\ max}$) is 6.8×10^{-3}, which is much less than the strain that would cause tensile rupture. Beyond the formation of the local buckle, pipe deformation concentrates around the buckled cross-section and the localized wrinkling pattern is further developed. Further continuation of the imposed deformation results in pipe wall folding, which is accompanied by significant local strains (compressive and tensile) at the buckled area. Moreover, the maximum tensile strain on the opposite (tensile) side of the pipe is also significantly increased.

Similarly, Figs. 23 and 24 present the results for an X65 steel pipeline with $D/t=72$, embedded in a more dense sand with values of ϕ and E equal to 40° and 50 MPa, respectively, referred to as "Sand II". The numerical results indicate that pipe bending deformation in Sand II occurs within a shorter distance from the fault location (5.1 m) due to the higher strength of this sand. Comparison of those results with the results in Figs. 21 and 22 demonstrates that for the same fault displacement d, higher bending stresses and strains occur in the case of Sand II. Local buckling occurs when the fault displacement becomes equal to 0.70 m, which is less than the corresponding critical fault displacement for the case of loose sand (0.87 m). The maximum

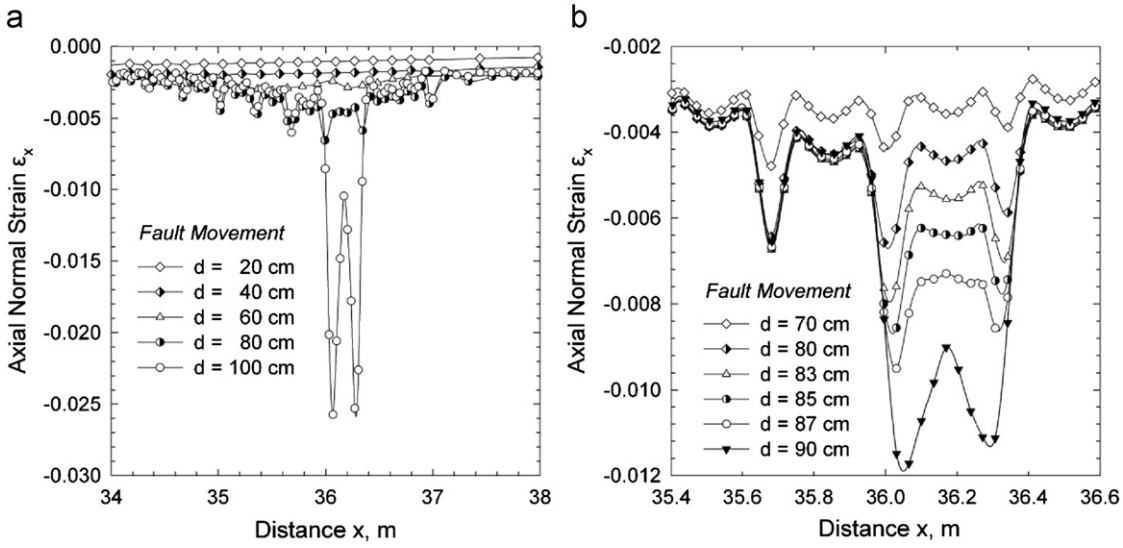

Fig. 21. Variation of axial strain at the compression side of the buckled area for different values of fault displacement (a) fault movement from 0.2 to 1.0 m and (b) fault movement from 0.70 to 0.90 m (X65 pipe, $D/t=72$, Sand I, $w=0.33$ m, $p=0$).

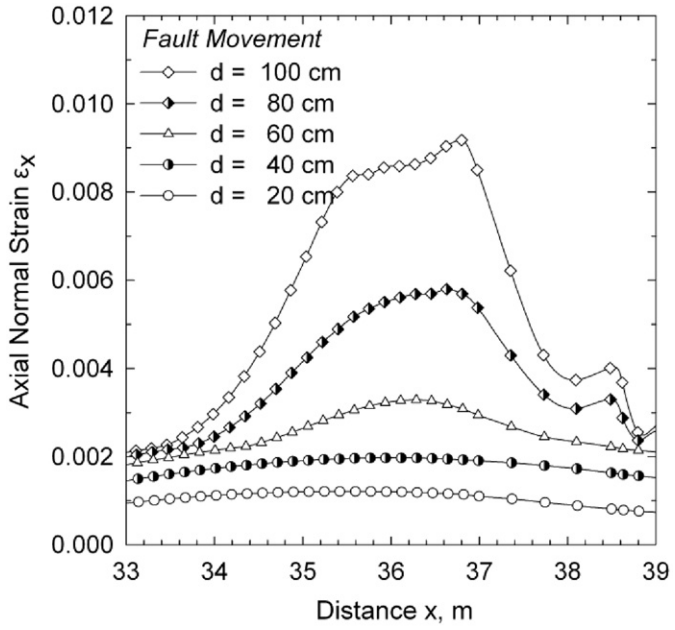

Fig. 22. Variation of axial strain at the tension side of the buckled area for different values of fault displacement from 0.2 to 1.0 m (X65 pipe, $D/t=72$, Sand I, $w=0.33$ m, $p=0$).

compressive strain ε_{cr} that causes local buckling is equal to 10.47×10^{-3}, whereas the corresponding maximum tensile strain $\varepsilon_{T,\,max}$ along the opposite generator is equal to 6.98×10^{-3}.

3.3. Effects of the diameter-to-thickness ratio and design implications

In order to investigate the effects of the diameter-to-thickness ratio, results are obtained for 36-in.-diameter X65 steel pipelines with thickness ranging between 1/4 and 3/4-in., corresponding to D/t values between 48 and 144. Both cohesive soils (Clay I and II) and non-cohesive soils (Sand I and II) are considered.

The numerical results for cohesive soils (Clay I and II) are summarized in Fig. 25. In particular, Fig. 25a plots the fault critical displacement, d_{cr}, normalized by the pipe diameter D, in terms of the diameter-to-thickness ratio, D/t. The results show a substantial decrease of d_{cr} with increasing value of the D/t ratio, which means that thin-walled pipelines are more prone to buckling and fail at relatively small values of fault displacement. Furthermore, stiff soil conditions result in significantly lower deformation capacity of the pipeline. In Fig. 25b the corresponding critical compressive strain at the onset of local buckling, ε_{cr}, is plotted against the value of the diameter-to-thickness ratio, D/t. The results indicate that thinner pipes buckle at smaller critical strain, which is in accordance with test data and numerical results from non-confined pipes [31–33].

In the above results, no critical displacement or critical strain is shown for $D/t=44$ and soft soil conditions (Clay I). In this particular case, the numerical results did not indicate local buckling; the pipeline exhibited significant ground-induced deformation without any wrinkling of the pipeline wall for fault displacements that exceed 2.5 m. The tensile strains developed in the pipeline due to longitudinal pipeline stretching are responsible for this behavior. Using a realistic approximation of the deformed shape of the pipeline, it is possible to develop a simplified analysis (see Appendix), which demonstrates the opposite effects of longitudinal bending and stretching, and results in the simple "no-buckling" condition equation (15). Adopting a value of α equal to 0.5 and assuming that $L/D\approx16$ for soft cohesive conditions (Clay I), as shown in Fig. 29 of the Appendix, then from equation (15), the limiting D/t value is equal to 53. This is somewhat higher than the D/t value of the pipeline under consideration ($D/t=44$), so that the "no-buckling" condition (15) is satisfied.

In Fig. 25b, the finite element results for the critical strain (ε_{cr}) are also compared with the predictions of the new European standard EN 1998-4 [35] for seismic design of buried pipelines, also adopted by the very recent ASCE Manual of Practice 119 for Buried Steel Pipes [36]. The EN 1998-4 standard specifies a maximum allowable strain for compression ($\varepsilon_{C,w}$) equal to the minimum of [0.01, $0.4t/D$] and a maximum allowable tensile strain ($\varepsilon_{T,w}$) equal to 0.03. The finite element results predict a decrease of the critical strain with increasing D/t values, which is in accordance with the provisions in [35,36]. However, it should be noticed that the allowable compressive strain appears to be conservative for the range of cohesive soil conditions expressed by Clay I and Clay II as shown in Fig. 25b.

Moreover, the numerical results of axial strain at the tension side of the pipe for all the cases considered in Fig. 25 show that at the onset of local buckling the computed maximum tensile strain

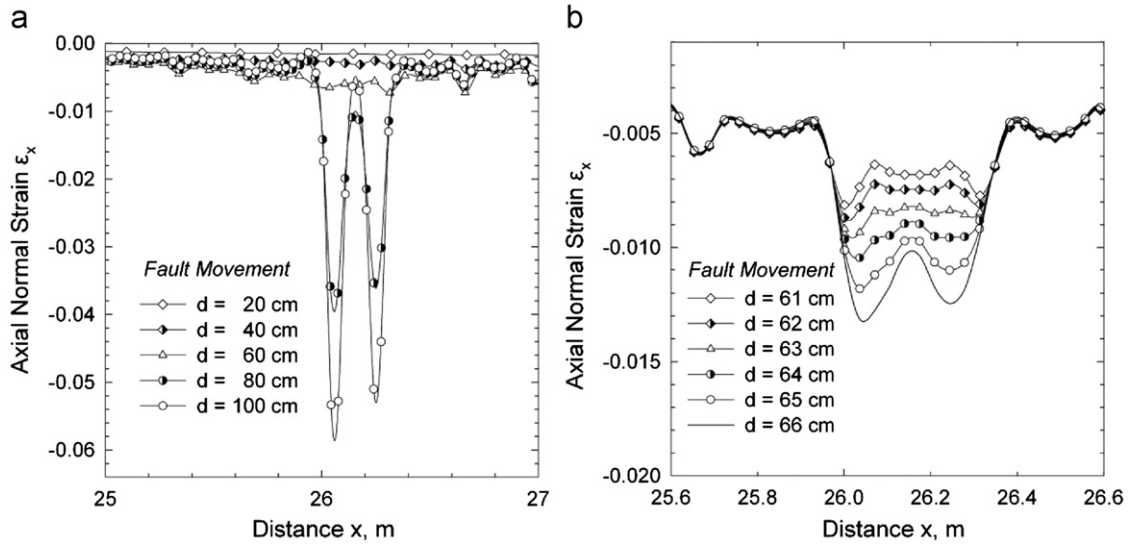

Fig. 23. Variation of axial strain at the compression side of the buckled area for different values of fault displacement: (a) fault movement from 0.2 to 1.0 m and (b) fault movement from 0.60 to 0.75 m (X65 pipe, $D/t=72$, Sand II, $w=0.33$ m, $p=0$).

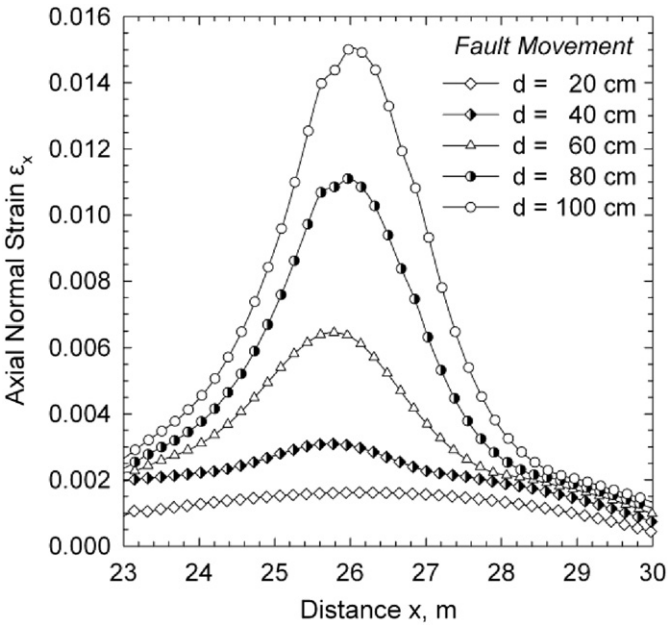

Fig. 24. Variation of axial strain at the tension side of the buckled area for different values of fault movement from 0.2 to 1.0 m (X65 pipe, $D/t=72$, Sand II, $w=0.33$ m, $p=0$).

$\varepsilon_{T,\,max}$ varies from 0.002 to 0.01, which is significantly lower than the EN 1998-4 allowable value of $\varepsilon_{T,w}=0.03$. This observation verifies that for the range of parameters considered in the present study, local buckling rather than tensile rupture is the governing mode of pipeline mechanical response.

In Fig. 25, the effects of internal pressure are also depicted. The numerical results are obtained for a pressure level equal to 56% of the maximum operating pressure, p_{max}, and show that the presence of internal pressure results in a small decrease of critical fault movement, d_{cr} in Fig. 25a, due to the additional stresses and strains in the pipeline wall because of pressure. Furthermore, the corresponding critical strain in the presence of pressure is similar to the corresponding critical strain for the zero pressure case, as shown in Fig. 25b. Note that EN 1998-4 provisions [35] specify a value of critical strain independent of the level of internal pressure, and this is in accordance with the present numerical results.

Finally, the numerical results for the mechanical behavior of X65 pipelines in non-cohesive soils (Sand I and II) are summarized in Fig. 26, in terms of the normalized fault critical displacement and the critical corresponding strain at buckling with respect to the diameter-to-thickness ratio, D/t. The results shown in Fig. 26a indicate that dense soil conditions (Sand II) result in lower deformation capacity of the pipeline. Furthermore, for both ground conditions, the critical compressive strain, ε_{cr}, shown in Fig. 26b, is significantly higher than the one predicted by the provisions of EN 1998-4 [35].

3.4. Structural behavior of high-strength X80 steel pipelines

The behavior of buried high-strength steel (API X80) pipelines under fault-induced deformation is also analyzed, using the numerical tools described in the previous sections. The nominal uniaxial tensile stress–strain relationship of the X80 material is plotted in Fig. 3b. The dashed material curve, which has a yield stress of 596 MPa and does not have a plastic plateau, corresponds to a cold expanded (UOE) pipe. The solid material curve with a yield stress of 550 MPa and a plastic plateau up to a strain of 1.48% represents a seamless steel pipe material. Results are obtained for 36-in.-diameter X80 steel pipelines with D/t ratios between 48 and 144.

Fig. 27a plots the value of the fault critical displacement, d_{cr}, normalized by the pipe diameter D, in terms of the diameter-to-thickness ratio, D/t, for the two types of X80 steel (shown in Fig. 3b) and for cohesive soil conditions (Clay I and II). As in the case of X65, the value of d_{cr} decreases significantly with increasing value of D/t, indicating that thin-walled pipelines are more vulnerable to buckling and may fail at relatively small values of fault displacement. It should be noted that for the softer Clay I material, no values of d_{cr} are given for $D/t=44$ and 72, as no wrinkling of the pipeline wall was observed in this case even for fault displacements exceeding 4 m. This is attributed to the beneficial effect of tensile deformation on the mechanical behavior of those relatively thick pipes, as described in the Appendix. Naturally, the values of d_{cr} for the high-strength steel X80 pipes in Fig. 27a are higher than those for the X65 pipes given in Fig. 25a. Similarly, Fig. 27b plots the corresponding critical axial strain, ε_{cr}, versus the diameter-to-thickness ratio, D/t, for zero internal pressure. Also plotted in the figure is the

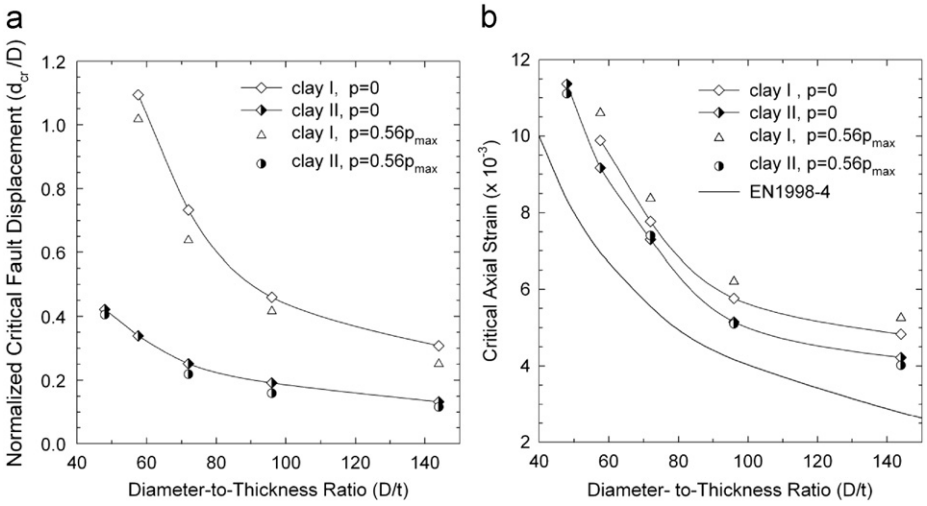

Fig. 25. (a) Critical fault movement versus the diameter-to-thickness ratio D/t for Clay I, II and (b) critical axial strain versus the diameter-to-thickness ratio D/t for clay I, II—predictions from EN 1998-4 (X65 pipe, $w=0.33$ m, $p=0$ and $p=0.56p_{max}$).

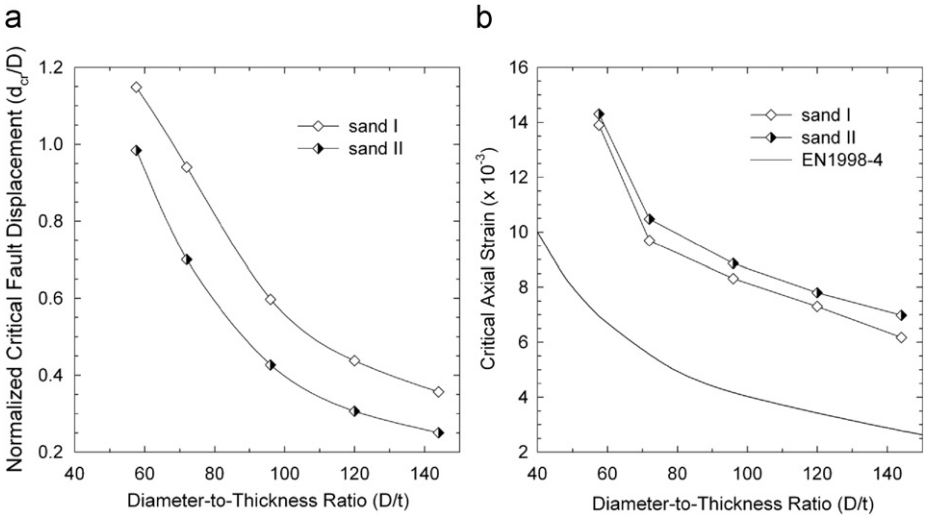

Fig. 26. (a) Critical fault movement versus the diameter-to-thickness ratio D/t for Sand I, II and (b) critical axial strain versus the diameter-to-thickness ratio D/t for Sand I, II—predictions from EN 1998-4 (X65 pipe, $w=0.33$ m, $p=0$).

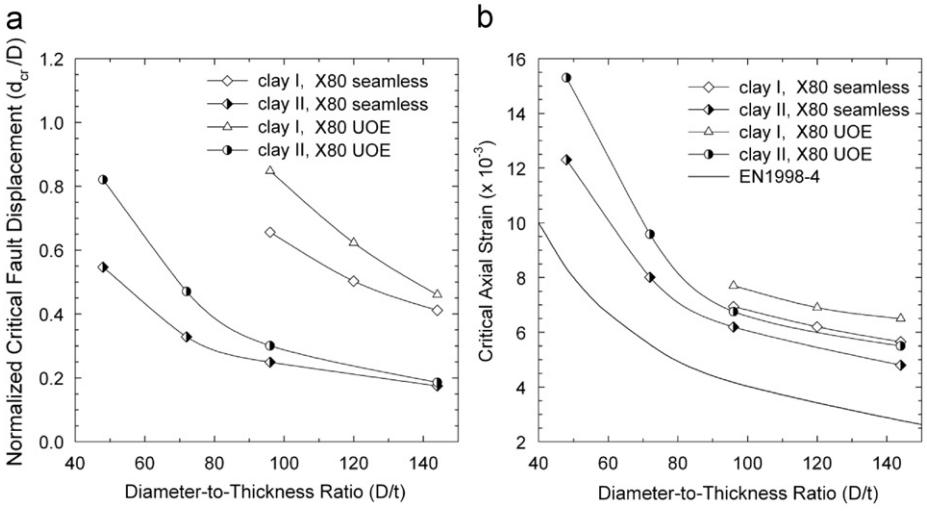

Fig. 27. (a) Critical fault movement versus the diameter-to-thickness ratio D/t for two different types of X80 pipelines and (b) Critical axial strain versus the diameter-to-thickness ratio D/t for two different types of X80—predictions from EN 1998-4 (X80 pipe, $w=0.33$ m, $p=0$).

recommendation by the EN 1998-4 giving more conservative values of ε_{cr}. Comparing the behavior of the two X80 materials, it is evident that both d_{cr} and ε_{cr} are higher for UOE pipe due to both increase of yield strength and higher initial post-yielding tangent modulus. The increase of buckling strength in UOE pipes is in accordance with the test data reported in [37,38].

Finally, the numerical results for the maximum axial strain ε_x at the tension side of the pipe at the onset of local buckling have been found to be significantly lower than the EN 1998-4 [35] allowable value of $\varepsilon_{T,w}=0.03$ for all values of D/t ratio examined in this paper.

4. Conclusions

Using advanced finite element simulation tools, the mechanical behavior of buried steel pipelines crossing an active strike-slip fault was investigated. The pipeline is assumed horizontal and normal to the fault plane, an idealized case, which allows for the investigation of several soil and pipe parameters on pipeline deformation and strength. In particular, the effects of various cohesive and non-cohesive soil conditions (expressed through various values of soil cohesion, friction, and stiffness parameters (c, ϕ, E)) on the structural response of the pipe are examined, with particular emphasis on pipe wall failure due to wrinkling (local buckling) or rupture.

An extensive parametric study is conducted, and numerical results are obtained for various values of D/t ratio and for X65 and X80 steel pipelines. In the majority of the cases analyzed, it is shown that the formation of local buckling due to excessive compressive strains at the pipeline wall is the governing mode of failure. The numerical results are presented in diagram form for the critical fault displacement d_{cr} and the corresponding critical strain ε_{cr}, and indicate a strong dependence in terms of the pipeline diameter-to-thickness ratio D/t.

It is concluded that in cohesive soils, softer ground conditions result in a large deformation capacity of the pipeline, whereas stiff ground conditions decrease the critical fault displacement. Similarly, in non-cohesive soils, loose sand conditions results in larger values of critical fault displacement than in dense soil conditions. The width of the fault slip zone was found to have non-important effects for the mechanical behavior of the pipe. It was demonstrated that the presence of internal pressure results in a small decrease of the deformation capacity, due to early yielding of the steel material. It was also concluded that high-strength X80 steel pipelines have a greater deformation capacity than X65 pipelines. Furthermore, cold-formed UOE X80 pipes exhibit better behavior in terms of buckling than seamless X80 pipes due to strain hardening.

Furthermore, the numerical results show that thick-walled pipes may not exhibit buckling; in those pipelines wall fracture may occur due to the development of excessive tensile strains. A simple analytical model is developed for illustrating this behavior, resulting in a simple "no-buckling" condition, expressed by Eq. (15).

Finally, the results from the present study are compared with the provisions of recent design standards and recommendations of EN 1998-4 and ASCE MOP 119, and can be used for buried steel pipeline design purposes, in the framework of a strain-based pipeline design.

Acknowledgements

The research work in this paper was partially supported by the Foundation of Education and European Civilization, Athens, Greece, through a Doctorate Research Fellowship granted to Mr. Polynikis Vazouras. This contribution is gratefully acknowledged.

Appendix. Simplified calculation of compressive strain

It is possible to develop a simplified formulation for pipeline deformation under strike-slip fault normal to the pipe axis, to estimate under which conditions the compressive strains that develop in the pipeline wall may cause local buckling. Towards this purpose, the pipeline is assumed to deform in an S-shaped "shearing type" configuration, as shown in Fig. 28a. In the pre-buckling stage, the shape is smooth and free of local discontinuities. A shape function of the beam-type deformation of pipeline is assumed to be in the form:

$$u(x)=\frac{d}{2}\left(1-\cos\frac{\pi x}{L}\right) \tag{2}$$

where d is the fault-imposed displacement and L is the length of the S-shaped deformed pipeline segment at the initial (non-deformed) pipeline configuration, i.e. the length of the S-shaped curved part of the pipeline in the fault area, as shown in Figs. 2 and 28a. Fig. 28b compares the shape of the deformed pipeline segment derived by the numerical analysis for Clay I (X65 pipe, $D/t=72$, $w=0.33$ m) to the assumed mathematical shape given by Eq. (2), for a fault displacement equal to 0.6 m. The value of L decreases with increasing soil stiffness and increasing D/t ratio, as shown in dimensionless form in Fig. 29 for cohesive soil conditions. From Eq. (2), the maximum

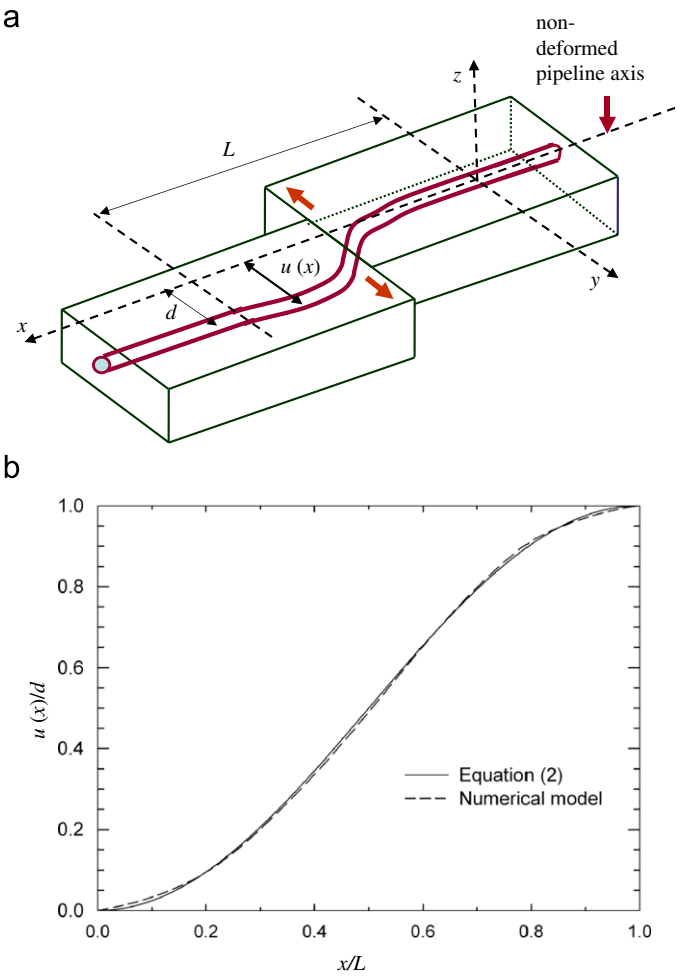

Fig. 28. (a) Assumed shape function $u(x)$ for pipeline longitudinal deformation; (b) comparison of the pipeline assumed shape at the onset of buckling from equation (2) and the finite element analysis (X65 pipe, $D/t=72$, Clay I, $w=0.33$ m, $p=0$, $d=0.6$ m).

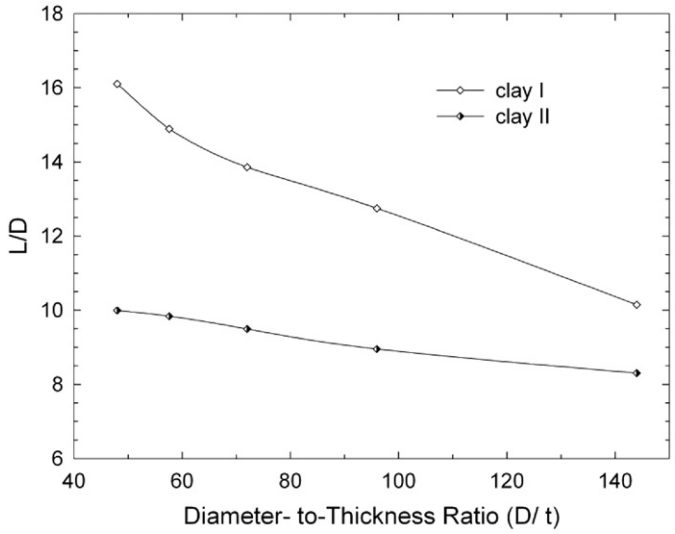

Fig. 29. Dimensionless length L/D versus the diameter-to-thickness ratio D/t for two different soil conditions (X65 pipe,$w=0.33$ m, $p=0$).

bending curvature k and the corresponding bending strain ε_b due to the imposed deformation d can be readily computed as follows:

$$k = -u''_{max} = \frac{d}{2}\left(\frac{\pi}{L}\right)^2 \tag{3}$$

$$\varepsilon_b = \frac{kD}{2} = \frac{\pi^2}{4}\left(\frac{d}{L}\right)\left(\frac{D}{L}\right) \tag{4}$$

Furthermore, the increase of pipeline length between cross-sections at $x=0$ and $x=L$ (pipeline stretching) is

$$\Delta = \int_0^L \sqrt{1+u'^2}\,dx - L \tag{5}$$

so that the corresponding axial strain (also referred to as "membrane" or "stretching" strain) ε_m is

$$\varepsilon_m = \frac{\Delta}{L} = \frac{1}{L}\int_0^L \sqrt{1+u'^2}\,dx - 1 \tag{6}$$

which is assumed to be uniformly distributed along the pipeline. Using the following series expansion:

$$\sqrt{1+u'^2} = 1 + \frac{1}{2}u'^2 + \cdots \tag{7}$$

and keeping only the first two terms, the axial membrane strain from Eq. (6) becomes

$$\varepsilon_m = \frac{\Delta}{L} \simeq \frac{1}{2L}\int_0^L u'^2\,dx = \frac{d^2\pi^2}{16L^2} \tag{8}$$

To compute the total axial compressive strain ε_C, the axial (tensile) membrane strain should be subtracted from the compressive bending strain. Combining Eqs. , one obtains the axial compressive strain at the critical location:

$$\varepsilon_C = \varepsilon_b - \varepsilon_m = \frac{\pi^2}{4L^2}\left(Dd - \frac{d^2}{4}\right) \tag{9}$$

The above equation shows that the total compressive strain consists of a linear part (due to bending) and a counteracting quadratic part (due to membrane axial tensile deformation). At the first stages of deformation, i.e. for small values of d, the membrane strain ε_m is small and the bending strain ε_b governs the response. On the other hand, the membrane strain ε_m becomes dominant at later deformation stages (large values of d). The value of fault displacement at which the compressive strain ε_C reaches a maximum value is readily obtained by differentiating equation (9):

$$\frac{d\varepsilon_C}{dd} = \frac{\pi^2}{4L^2}\left(D - \frac{d}{2}\right) \tag{10}$$

Setting the above derivative equal to zero, one obtains

$$d \equiv d_0 = 2D \tag{11}$$

so that the corresponding maximum value of compressive strain ε_C is

$$\varepsilon_{C,max} = \frac{\pi^2}{4}\left(\frac{D}{L}\right)^2 \tag{12}$$

Beyond that stage, the value of compressive strain ε_C decreases with increasing fault displacement d.

If the maximum axial compressive strain $\varepsilon_{C,\,max}$ in Eq. (12) is lower than the buckling (critical) strain ε_{cr} of the pipeline wall, local buckling may not occur. This is expressed mathematically as follows:

$$\varepsilon_{C,max} \le \varepsilon_{cr} \tag{13}$$

In the above equation, the buckling (critical) strain ε_{cr} can be written in the following form [35]:

$$\varepsilon_{cr} = \alpha\left(\frac{t}{D}\right) \tag{14}$$

where α is a constant that depends on the pipeline material grade, as well as the amplitude and shape of initial imperfections. Inserting Eqs. (12) and (14) into Eq. (13), one obtains the following "no-buckling" condition in terms of the diameter-to-thickness ratio D/t, the dimensionless parameter α and the length-over-diameter ratio L/D of the S-shaped deformed pipeline:

$$\frac{D}{t} \le \left(\frac{D}{t}\right)_{lim} = 0.4\alpha\left(\frac{L}{D}\right)^2 \tag{15}$$

The above expression shows that, in the case of strike-slip faults perpendicular to the pipeline axis, in order to avoid local buckling of the pipeline, the diameter-to-thickness ratio D/t should not exceed the limit value $(D/t)_{lim}$ given in Eq. (15). This limit value depends on the pipeline material (which influence the value of the dimensionless parameter α) and the soil conditions (which have a direct effect on the value of the L/D ratio).

Moreover, Eq. (15) can be employed to derive some useful qualitative results. More specifically, Eq. (15) indicates that steel pipelines embedded in relatively stiff soil conditions should be quite thick-walled (i.e. have a low value of D/t ratio) in order to avoid local buckling, whereas soft ground conditions relax this requirement. Furthermore, the use of high-strength steel for pipeline material (e.g. steel grade API 5L X80) results in an increase of parameter α, thus increasing pipeline ability to deform under ground-induced actions without the occurrence of local buckling.

References

[1] Ariman T, Muleski GE. A review of the response of buried pipelines under seismic excitations. Earthquake Engineering and Structural Dynamics 1981;9:133–51.
[2] Liang J, Sun S. Site effects on seismic behavior of pipelines: a review. ASME Journal of Pressure Vessel Technology 2000;122(4):469–75.
[3] Jennings, P.C., 1971. Engineering features of the San Fernando earthquake February 9, 1971, California Institute of Technology Report, EERL 71–02, Pasedena, CA.

[4] MaCaffrey MA, O'Rourke TD. Buried pipeline response to reverse faulting during the 1971 San Fernando Earthquake. ASME, PVP conference 1983;77: 151–9.
[5] Desmod TP, Power MS, Taylor CL, Lau RW. Behavior of large-diameter pipeline at fault crossings. ASCE, TCLEE 1995(6):296–303.
[6] Nakata T, Hasuda K. Active fault I 1995 Hyogoken Nanbu earthquake. Kagaku 1995;65:127–42.
[7] Earthquake Engineering Research Institute. Kocaeli, Turkey Earthquake of August 17. EERI Special Earthquake Report, 1999.
[8] Takada S, Nakayama M, Ueno J, Tajima C. Report on Taiwan Earthquake. RCUSS, Earthquake Laboratory of Kobe University, 1999. p. 2–9.
[9] Newmark NM, Hall WJ. Pipeline design to resist large fault displacement. In: Proceedings of U.S. national conference on earthquake engineering, 1975. p. 416–25.
[10] Kennedy RP, Chow AW, Williamson RA. Fault movement effects on buried oil pipeline. ASCE Journal of Transportation Engineering 1977;103:617–33.
[11] Kennedy, R.P., Kincaid,, R.H. . Fault crossing design for buried gas oil pipelines. ASME, PVP conference 1983;77:1–9.
[12] Wang LRL, Yeh YA. A refined seismic analysis and design of buried pipeline for fault movement. Earthquake Engineering and Structural Dynamics 1985;13:75–96.
[13] Vougioukas EA, Theodossis C, Carydis PG. Seismic analysis of buried pipelines subjected to vertical fault movement. ASCE Journal of Technical Councils 1979;105(TCI):432–441.
[14] Wang LLR, Wang LJ. Parametric study of buried pipelines due to large fault movement. ASCE, TCLEE 1995 1995(6):152–9.
[15] Takada S, Hassani N, Fukuda K. A new proposal for simplified design of buried steel pipes crossing active faults. Earthquake Engineering and Structural Dynamics 2001;30:1243–57.
[16] Kokavessis NK, Anagnostidis GS. Finite element modelling of buried pipelines subjected to seismic loads: soil structure interaction using contact elements. In: Proceedings, ASME PVP conference, Vancouver, BC, Canada, 2006.
[17] Karamitros DK, Bouckovalas GD, Kouretzis GP. Stress analysis of buried steel pipelines at strike-slip fault crossings. Soil Dynamics and Earthquake Engineering 2007;27:200–11.
[18] Liu M, Wang, Y-Y, Yu Z. Response of pipelines under fault crossing. In: Proceedings, international offshore and polar engineering conference, Vancouver, BC, Canada, 2008.
[19] Ha D, Abdoun TH, O'Rourke MJ, Symans MD, O'Rourke TD, Palmer MC, et al. Buried high-density polyethylene pipelines subjected to normal and strike-slip faulting—a centrifuge investigation. Canadian Geotechnical Journal 2008;45: 1733–42.
[20] Ha D, Abdoun TH, O'Rourke MJ, Symans MD, O'Rourke TD, Palmer MC, et al. Centrifuge modeling of earthquake effects on buried high-density polyethylene (HDPE) pipelines crossing fault zones. ASCE Journal of Geotechnical and Geoenvironmental Engineering 2008;134(10):1501–15.
[21] Abdoun TH, Ha D, O'Rourke MJ, Symans MD, O'Rourke TD, Palmer MC, et al. Factors influencing the behavior of buried pipelines subjected to earthquake faulting. Soil Dynamics and Earthquake Engineering 2009;29:415–27.
[22] Lillig DB, Newbury BD, Altstadt SA. The second ISOPE strain-based design symposium—a review. In: Proceedings of the international society of offshore and polar engineering conference, Osaka, Japan, 2009.
[23] ABAQUS. Users' manual, version 6.7. Providence, RI, USA: Simulia; 2008.
[24] Mohitpour M, Golshan H, Murray A. Pipeline design & construction: a practical approach. third ed.. New York, NY: ASME Press; 2007.
[25] Anastasopoulos I, Callerio A, Bransby MF, Davies MC, Nahas AEl, Faccioli E, et al. Numerical analyses of fault foundation interaction. Bulletin of Earthquake Engineering 2008;6(4):645–75.
[26] Gazetas G, Anastasopoulos I, Apostolou M. Shallow and deep foundation under fault rapture or strong seismic shaking. In: Pitilakis K, editor. Earthquake Geotechnical Engineering. Springer; 2007. p. 185–215.
[27] Bransby MF, Davies MC, Nahas AEl. Centrifuge modeling of normal fault-foundation interaction. Bulletin of Earthquake Engineering 2008;6(4):585–605.
[28] American Petroleum Institute. Specification for line pipe, 44th ed. ANSI/API Spec 5L, 2007.
[29] American Society of Mechanical Engineers. Pipeline transportation systems for liquid hydrocarbons and other liquids. ANSI/ASME 2006;B31:4.
[30] American Society of Mechanical Engineers. Gas transmission and distribution piping systems. ANSI/ASME 2007;B31:8.
[31] Gresnigt AM. Plastic design of buried steel pipes in settlement areas. HERON 1986;31(4):1–113.
[32] Kyriakides S, Ju GT. Bifurcation and localization instabilities in cylindrical shells under bending I: experiments. International Journal of Solids and Structures 1992;29:1117–42.
[33] Limam A, Corona E, Lee L-H, Kyriakides S. Inelastic wrinkling and collapse of tubes under combined bending and internal pressure. International Journal of Mechanical Sciences, in press (available online).
[34] Igi S, Suzuki, N. Tensile strain limits of X80 high-strain pipelines. In: Proceedings of the 16th international offshore and polar engineering conference, Lisbon, Portugal, 2007.
[35] Comité Européen de Normalisation. Eurocode 8, Part 4: Silos, tanks and pipelines. CEN EN 1998-4, Brussels, Belgium, 2006.
[36] American Society of Civil Engineers. Buried flexible steel pipe; design and structural analysis. In: Whidden WR, editor. ASCE Manual of Practice, MOP; 2009. p. 119.
[37] Gresnigt AM, van Foeken RJ. Local buckling of UOE and seamless steel pipes. In: Proceedings of the 11th international offshore and polar engineering conference, Stavanger, Norway, vol. II, 2000. p. 131–42.
[38] Gresnigt AM, Karamanos SA. Local buckling strength and deformation capacity of pipes. In: Proceedings of the 19th International Offshore and Polar Engineering Conference, Osaka, Japan, 2009. p. 212–23.